Effects of Sequential Ligation of Molybdenum Cation by Chalcogenides on Electronic Structure and Gas-Phase Reactivity†

Ilona Kretzschmar, Andreas Fiedler,‡ Jeremy N. Harvey, Detlef Schröder, and Helmut Schwarz*

Institut für Organische Chemie der Technischen, Universität Berlin, Strasse des 17. Juni 135, D-10623 Berlin, Germany

Received: June 13, 1997⊗

The molybdenum chalcogenide cations MoX_n^+ (X = O, S; $n = 1-3$) are studied by a combined experimental and theoretical approach. The monoligated species MoO^+ and MoS^+ both have ($^4\Sigma^-$) ground states that formally arise from spin-pairing of Mo^+ (^{6}S) with O (^{3}P) and S (^{3}P), respectively. Similarly, the bent triatomic MoX_2^+ cations exhibit doublet ground states ($^2A_1$). The trichalcogenides MoO_3^+ and MoS_3^+ also have doublet ground states and exhibit similar C_{3v}-symmetrical structures; however, distinct energetic differences are found in that MoO_3^+ is much less stable than MoS_3^+, due to the necessity to ionize a strong Mo−O double bond in neutral MoO_3. Sequential addition of chalcogenides to molybdenum goes hand in hand with an increase of the formal oxidation state of the metal. As a result, the ionization energies (IEs) increase with the electronegativity and the number of the chalcogenide atoms added: IE(MoO) = 7.9 ± 0.3 eV, IE(MoO_2) = 8.7 ± 0.3 eV, IE(MoO_3) = 11.7 ± 0.3 eV, IE(MoS) = 7.7 ± 0.3 eV, IE(MoS_2) = 8.6 ± 0.3 eV, and IE(MoS_3) = 8.9 ± 0.3 eV. Thermochemical considerations in conjunction with the ion/molecule reaction bracketing technique and theoretical results provide reevaluated values for the bond dissociation energies (in kcal/mol): Mo^+−O 118 ± 2, OMo^+−O 131 ± 5, O_2Mo^+−O 62 ± 17, Mo^+−S 88 ± 14, SMo^+−S 100 ± 14, and S_2Mo^+−S 88 ± 14. Notable differences are observed in the gas-phase reactivity of the MoX_n^+ cations. In general, the molybdenum sulfides are less reactive than the corresponding oxides. The monoligated MoX^+ cations promote C−H bond activation of hydrocarbons, while the MoX_2^+ cations and also MoS_3^+ are somewhat less reactive. The high-valent transition-metal oxide MoO_3^+ is the most reactive species and is even capable of activating methane.

Introduction

Molybdenum is one of the essential elements in biology. It serves central functions in redox enzymes of the human body[1] and is involved in mixed Mo/Fe sulfide clusters, which are essential for nitrogen fixation by prokaryotic organisms.[2] Further, molybdenum chalcogenides play a role in various industrial processes.[3] Therefore, the examination of Mo−chalcogenide interactions and the synthesis of model compounds attract continued attention.[4]

The gas-phase chemistry of molybdenum deserves interest because it can provide insight into the intrinsic properties of the element and unravel features associated with its reactivity when ligated to chalcogenides. The gas-phase chemistry of bare Mo^+ cations has so far only scarcely been studied,[5] primarily due to the fact that Mo^+ is nonreactive toward most substrates. This lack of reactivity has been attributed to the inertness of the $5s^04d^5$ configuration of the Mo^+ (^{6}S) ground state.[6] Recently, the gas-phase chemistry of MoO_n^+ ($n = 0-2$) has been examined by Cassady and McElvany,[7,8] and in comparison to bare Mo^+, the metal-oxide cations MoO^+ and MoO_2^+ are more efficient as far as C−H and C−C bond activation of hydrocarbons is concerned.

Here, we report a combined experimental and computational study of MoX_n^+ cations (X = O, S; $n = 1-3$) with respect to the electronic ground states, the nature of the bonding, the energetics of these species, and their reactivity toward selected organic substrates. In addition, the associated thermochemistry of the MoX_n^+ systems is evaluated by means of adequate computational methods and the ion/molecule reaction bracketing technique.

Experimental and Computational Methods

The experiments were performed in a Spectrospin-CMS-47X Fourier-transform ion-cyclotron resonance (FTICR) mass spectrometer equipped with an external ion source that has been described elsewhere.[9] Briefly, Mo^+ ions were generated *via* laser desorption/laser ionization by focusing the beam of a Nd:YAG laser (Spectron Systems, $\lambda = 1064$ nm) onto a target of pure molybdenum. The ions were extracted from the source and transferred into the analyzer cell by a system of electrostatic potentials and lenses. After deceleration, the ions were trapped in the field of a superconducting magnet (maximum field: 7.05 T). The most abundant isotope $^{98}Mo^+$ was isolated from the other isotopes using FERETS,[10] a computer-assisted protocol that combines frequency sweeps and single-frequency ion-ejection pulses to optimize ion isolation. Generation of the MoX_n^+ ions was achieved as follows: (i) sequential oxidation of Mo^+ with pulsed-in O_2 yields MoO^+ and MoO_2^+, (ii) MoO_3^+ was generated by reacting Mo^+ with a *ca.* 1:5 mixture of O_2 and N_2O, and (iii) MoS_n^+ ($n = 1-3$) species were prepared by sequential sulfur-atom transfer to Mo^+ with carbonyl sulfide as reagent gas. The ions under investigation were then again isolated using FERETS. For MoS^+, we faced the problem of coincidental mass overlap, because isobaric MoO_2^+ was also present due to reaction of Mo^+ with residual air in the mass spectrometer. In order to avoid unintentional excitation of MoS^+, the MoO_2^+ ions were therefore not ejected in these

† Dedicated to Professor Peter C. Thieme, BASF Ludwigshafen, on the occasion of his 60th birthday.

‡ Present address: Institute for Molecular Sciences, Myodaiji, 444 Okasaki, Japan.

⊗ Abstract published in *Advance ACS Abstracts,* August 1, 1997.

S1089-5639(97)01941-5 CCC: $14.00

experiments. Instead of this, high-resolution mass spectra were acquired at different reaction times and used for the correction of the results for the interfering MoO_2^+ species. In general, for the purpose of thermalization and removal of excess energy, the ions were collided with pulsed-in methane (maximum pressure ca. 5×10^{-5} mbar, ca. 2000 collisions). In the case of MoO_3^+ this was impossible, because this ion reacts with methane (see below); therefore, the O_2/N_2O mixture and argon were used instead. The kinetics of all reactions were carefully studied as a function of thermalizing collisions in order to ensure that the ions undergoing ion/molecule reactions were not kinetically and/or electronically excited. The reactants were admitted to the cell through leak valves at stationary pressures of $(0.6-4.0) \times 10^{-8}$ mbar (as measured by a Balzers IMG070 ion gauge). Some of the ions under study, in particular MoO_3^+, react rapidly with water, which is inevitably present in the background of the vacuum system; others, such as for instance MoS^+, show reactivity toward the residual air in the FTICR. Therefore, the background reactions were measured separately and subtracted from the data obtained in the presence of a given substrate. The first-order kinetics of the reacting ions provided the rate constants k_{exp}, which were compared to the gas-kinetic collision rates k_{ADO}.[11] Due to the evaluation of the data via background correction, the accuracy of the rate constants was not better than ±50%. Further, note that the reaction kinetics were only analyzed in terms of the first-order formalism, and radiative and/or collisional stabilization of the encounter complexes resulting in adduct formation was neglected.[12] In the thermochemical analysis of some ion/molecule reactions (bracketing technique), we took into account the circumstances under which reactions occur under FTICR conditions when the reactant ions are properly thermalized; thus, endothermic reactions do not occur if the reaction enthalpy (ΔH_R) exceeds ca. 5 kcal/mol. For reactions with ΔH_R between +5 and −5 kcal/mol, the reaction rates increase from $<10^{-13}$ cm^3 s^{-1} molecule^{-1} to the collision limit as a function of exothermicity if no kinetic restrictions apply.[13] The rate constants allow refined estimates for the thermochemistry of a given reaction, assuming that no kinetic barriers are operative; at least for electron transfer processes, the latter assumption appears to be quite reasonable. However, for transition-metal cations the bracketing technique is usually limited to an accuracy of ±5 kcal/mol, due to the occurrence of association or competing side reactions.

Similar to our previous studies of transition-metal dioxides,[14] the computational study of the MoX_n^+ systems for X = O and S was performed in the following way: The geometries were optimized using the Becke3LYP functional,[15] a density functional theory (DFT) approach implemented in the GAUSSIAN92/DFT[16] program; this will be referred to as B3LYP. At this level of theory, the stationary points were characterized as minima on the potential-energy surface by evaluating their vibrational frequencies and normal modes using analytically derived first derivatives and numerically calculated force-constant matrices. For MoO^+ and MoS^+ the B3LYP geometries were reoptimized at the CASSCF and CASPT2D[17] levels of theory by employing the MOLCAS version 3 program package.[18] Due to the minor changes in geometries upon switching the level of theory (ca. 0.02 Å, including relativistic bond contraction),[19] this costly procedure was omitted for the larger oxides and sulfides, and the B3LYP geometries were used for CASSCF and CASPT2D energy calculations. In the CAS calculations the active space included the 4d and 5s orbitals of molybdenum and the 2p and the 3p orbitals of oxygen and sulfur, respectively. Inclusion of the 2s and 3s orbitals, respectively, of the chalcogenides in the active space decreases the computed total energies by 0.6 and 0.9 kcal/mol for MoO^+ and MoS^+.[19] This approach could not be extended to the dichalcogenides, because the MOLCAS version 3 program cannot treat more than 12 orbitals in the active space, such that inclusion of the 2s and 3s orbitals, respectively, is prevented for MoX_2^+ (X = O, S). All electrons were correlated at the CASPT2D level of theory. A first-order correction of the energies with respect to the relativistic effects[20] was achieved by computation of the mass-velocity and Darwin terms at the CASSCF level. These relativistic corrections were added to the B3LYP, CASSCF, and CASPT2D energies, which will be referred to as B3LYPrel, CASrel, and CASPT2Drel, respectively. Treatment of the trioxide and the trisulfide at the CAS level of theory with reasonably sufficient basis sets would require outrageous computational resources and was therefore not attempted.

In the B3LYP approach, Dunning/Huzinaga full double-ξ basis sets[21] with polarization functions were employed for O and S, while atomic natural orbital (ANO) basis sets[22] were used for these atoms in the CASSCF and CASPT2D calculations. Throughout this study an all-electron basis set (17s13p9d3f)/[7s6p4d1f][23] was used for molybdenum. Calculation of the first and second ionization energies of molybdenum gave 7.2 (exptl 7.09) and 16.2 (exptl 16.15) eV, respectively, at the CASPT2Drel level of theory. However, these basis sets as well as the active space are by no means complete, and these restrictions have to be kept in mind in the discussion of the theoretical results. Bond dissociation energies (BDEs) were derived from the sum of energies of the isolated molecules and atoms without any further corrections. For the purpose of better understanding the electronic structures in terms of molecular orbital theory, the CAS wave functions and the associated MOs were computed and graphically illustrated using the GAMESS program package.[24] All computations were performed on either IBM/RS 6000 workstations or a CRAY-YMP computer.

Results and Discussion

This part is divided in three sections. First, the molybdenum-oxide cations MoO_n^+ ($n = 1-3$) are described with respect to their genesis, the associated thermochemistry, geometrical and electronic features, and the ground-state configurations. For the evaluation of the gas-phase reactivities, the hydrocarbons methane, ethane, benzene, and toluene were chosen as model substrates. Then follows a discussion of the molybdenum sulfide cations MoS_n^+ ($n = 1-3$). Finally, the results for cationic molybdenum oxides and sulfides are compared with each other in order to illustrate the differences and similarities in the chemical behavior of these metal chalcogenides.

Molybdenum Oxide Cations MoO^+, MoO_2^+, and MoO_3^+. *Generation and Thermochemistry of MoO_n^+ ($n = 1-3$).* Molybdenum monoxide and dioxide cations can be generated from thermalized Mo^+ and oxygen in the sequential reactions 1 and 2. Formation of the molybdenum trioxide cation is impossible *via* this route, i.e. reaction 3, and requires the use of dinitrogen oxide as oxidant; for convenience, a mixture of O_2 and N_2O was used to generate MoO_3^+ directly from Mo^+.

$$Mo^+ + O_2 \rightarrow MoO^+ + O \quad (1)$$

$$MoO^+ + O_2 \rightarrow MoO_2^+ + O \quad (2)$$

$$MoO_2^+ + O_2 \rightarrow MoO_3^+ + O \quad (3)$$

The occurrence of reactions 1 and 2 for thermalized ions implies that BDE(Mo^+-O) and BDE(OMo^+-O) are similar

to BDE(O−O) = 119 kcal/mol[25] or even exceed it; the absence of O-atom transfer from O_2 to MoO_2^+ in reaction 3 suggests that BDE(O_2Mo^+−O) < 119 kcal/mol, provided no kinetic barrier exists.

For MoO^+ we can derive a more precise BDE from the fact that the rate constant of reaction 1 is significantly lower than the collision limit ($k_{exp}/k_{ADO} = 0.18$). Considering that O-atom abstraction from triplet dioxygen is unlikely to be associated with a large barrier, we can assume that the low efficiency of reaction 1 reflects its endothermicity and thus apply the Arrhenius equation,[13,26] resulting in BDE(Mo^+−O) = 118 ± 2 kcal/mol. An alternative way to evaluate BDEs is the use of thermochemical cycles. For that purpose, we determined the ionization energy of MoO by the bracketing method: When MoO^+ is reacted with aniline (IE = 7.72 eV[25]), rapid electron transfer (ET) occurs to yield the aniline cation radical concomitant with neutral MoO, whereas in the reaction of MoO^+ with cycloheptatriene (IE = 8.29 eV[25]) ET does not take place at all. Considering the requirements for observation of an ion/molecule reaction under FTICR conditions,[13] these ET-results lead to an estimate of IE(MoO) = 7.9 ± 0.3 eV. In order to evaluate the thermochemistry of neutral MoO, we combined the literature values of $\Delta H_f°$(MoO) = 74 ± 8 kcal/mol[27] and 83 ± 5 kcal/mol[28] to an average, i.e. $\Delta H_f°$(MoO) = 79 ± 8 kcal/mol. Together with $\Delta H_f°$ of Mo and O as well as IE(Mo), these data lead to BDE(Mo^+−O) = 119 ± 15 kcal/mol.

Although within the experimental error limits, both values derived in this work are slightly higher than the literature reference of BDE(Mo^+−O) = 113 ± 18 kcal/mol,[25] due to the different IE(MoO) and $\Delta H_f°$(MoO) used. This literature value is however inconsistent with the occurrence of reaction 1 for thermalized Mo^+, which proceeds until complete conversion of the metal cation. We therefore recommend BDE(Mo^+−O) = 118 ± 2 kcal/mol as a reevaluated value. Quite recently we learned about an experimental value of 116.7 ± 1.4 kcal/mol,[29] which is in pleasing agreement with our evaluation. Cassady and McElvany[7] have already argued that the literature value for BDE(Mo^+−O) may be too small due to the failure to observe reaction 4 under FTICR conditions.

$$MoO^+ + H_2 \not\rightarrow Mo^+ + H_2O \qquad (4)$$

$$Mo^+ + H_2O \not\rightarrow MoO^+ + H_2 \qquad (5)$$

Although these authors used an entirely different method for the generation of MoO_n^+ cations (i.e. laser ablation of molybdenum oxide pellets), the present experiments fully confirm the nonoccurrence of reaction 4; however, the reverse reaction 5 also does not take place with a measurable rate constant ($k < 10^{-13}$ cm^3 s^{-1} molecule^{-1}). Failure to observe either reaction highlights the ambiguity inherent in deriving thermochemical quantities from the absence of certain ion/molecule reactions. In fact, according to the BDE(Mo^+−O) derived in this study, both reactions should occur at room temperature if they were controlled by thermochemistry alone. In reality, however, bond activations of molecular hydrogen or water, respectively, are often associated with substantial barriers en route to the products that may prevent reactions 4 and 5 from taking place under thermal conditions. In general, for the first-row transition metals M most bare metal cations M^+ as well as the oxide cations MO^+ exhibit such barriers in the reactions with H_2O and H_2, respectively; these findings can be attributed to geometrical constraints in the cyclic transition structures in conjunction with crossings of different spin state surfaces along the reaction coordinates.[26,30−32]

For molybdenum dioxide cation, the occurrence of reaction 2 with unit efficiency provides a lower limit of BDE(OMo^+−O) > 119 kcal/mol. Further thermochemical information is gained from the examination of reaction 6:

$$MoO^+ + CO_2 \rightarrow MoO_2^+ + CO \qquad (6)$$

The fact that O-atom transfer from carbon dioxide to MoO^+ can take place requires that BDE(OMo^+−O) is close to or even exceeds BDE(OC−O) = 127 kcal/mol. The rate constant of reaction 6 is extremely small ($k_{exp}/k_{ADO} = 0.001$), indicating that reaction 6 is slightly endothermic and/or associated with a significant barrier. However, reduction of MoO_2^+ by CO does not take place; thus, reaction 6 is exothermic, suggesting BDE(OMo^+−O) ≥ 127 kcal/mol. Bracketing of the IE(MoO_2) with cycloheptatriene (rapid ET, IE =7.29 eV[25]), toluene (slow ET, IE = 8.82 eV[25]), and benzene (no ET, IE = 9.25 eV[25]) leads to IE(MoO_2) = 8.7 ± 0.3 eV; again, this ionization energy is somewhat lower than the previous value of IE(MoO_2) = 9.2 eV,[25] thus resulting in a larger BDE(OMo^+−O) as compared to the older literature value of 113 kcal/mol.[25] Combination with $\Delta H_f°(MoO_2) = -2 \pm 3$ kcal/mol[27] and BDE(Mo^+−O) = 118 ± 2 kcal/mol as derived above leads to BDE(OMo^+−O) = 122 ± 13 kcal/mol, and by incorporating the results for reactions 2 and 6, respectively, we arrive at BDE(OMo^+−O) = 131 ± 5 kcal/mol. The interesting aspect that BDE(OMo^+−O) exceeds BDE(Mo^+−O) by ca. 10 kcal/mol will be discussed further below in the context of the theoretical results.

The failure to form MoO_3^+ in reaction 3 suggests an upper limit for BDE(O_2Mo^+−O) < 119 kcal/mol. Vice versa, a lower limit of BDE(O_2Mo^+−O) > 40 kcal/mol can be obtained from the formation of MoO_3^+ upon reaction of MoO_2^+ with N_2O. A more narrow bracket of 40 kcal/mol < BDE(O_2Mo^+−O) < 90 kcal/mol can be obtained from the reaction of MoO_3^+ with methane (see below); unfortunately, further refinement was not possible due to the lack of thermochemical data for an evaluation of the energetics of the other reactions of MoO_3^+. From the observation of ET from ethyne (IE = 11.4 eV[25]) to MoO_3^+, and its complete absence in the presence of O_2 (IE = 12.1 eV[25]), the IE(MoO_3) can roughly be bracketed as 11.7 ± 0.3 eV, which practically coincides with the literature value;[25] refinement of the ET bracket was impossible as appropriate reagents with IEs between 11.4 and 12 eV were not available. Combination of the IE with $\Delta H_f°(MoO_3) = -82 \pm 5$ kcal/mol and the thermochemistry derived above for MoO_2^+ leads to BDE(O_2Mo^+−O) = 62 ± 17 kcal/mol.

Computational Study of the MoO_n^+ System. Molybdenum cation has a ^{6}S ground-state corresponding to a $5s^04d^5$ configuration of the valence shell.[33] Perfect pairing of Mo^+ (^{6}S) and the ^{3}P ground state of an oxygen atom gives rise to a quartet state for MoO^+; spin flipping may also allow for doublet and sextet states. The density functional theory calculations with B3LYP predict the doublet state MoO^+ ($^2\Delta$) as the electronic ground state, which is 7.2 kcal/mol more stable than the quartet state MoO^+ ($^4\Sigma^-$) (Table 1). At the CASSCF and CASPT2D levels, however, MoO^+ ($^4\Sigma^-$) is the electronic ground state, while MoO^+ ($^2\Delta$) is higher in energy by 1.2 and 6.3 kcal/mol, respectively. This difference is further pronounced by relativistic effects, and according to the CASPT2Drel calculations, MoO^+ ($^4\Sigma^-$) is 17.2 kcal/mol more stable than MoO^+ ($^2\Delta$). Further, unlike the quasi-degeneracy of the $^4\Sigma$ and $^4\Pi$ states in the lower congener CrO^+ ($\Delta E \approx 2$ kcal/mol),[34] the two quartet states MoO^+ ($^4\Sigma^-$) and MoO^+ ($^4\Pi$) are well separated with the $^4\Pi$ state lying 13.5 kcal/mol higher in energy at the CASPT2Drel level. The possibility of a sextet ground state for MoO^+ can

TABLE 1: Geometries and Total Energies (hartree)[a] of Different Electronic States of MoO_n^+ ($n = 0-3$)

	state	geometry[b,c]			B3LYP	CAS	CASrel	CASPT2D	CASPT2Drel
		r_{Mo-O}	r_{Mo-O}	β_{O-Mo-O}					
Mo^+	^6S				−3977.229 37	−3975.238 35	−4042.873 89	−3975.513 90	−4043.149 44
MoO^+	$^2\Delta$	1.61			−4052.483 03	−4050.167 62	−4117.868 33	−4050.614 09	−4118.314 80
	$^4\Sigma^-$	1.64			−4052.471 58	−4050.169 61	−4117.887 62	−4050.624 18	−4118.342 19[d]
	$^6\Sigma^-$	1.64			−4052.288 32[e]	−4050.008 02	−4117.722 40	−4050.495 84	−4118.210 22
MoO_2^+	$^2A_1$	1.67	1.67	108.6	−4127.751 96	−4125.137 47	−4192.908 85	−4125.787 05	−4193.558 43[f]
	$^4A_2$	1.67	1.67	108.6	−4127.659 94[g]	−4125.028 02	−4192.798 57	−4125.699 65	−4193.470 20[h]
MoO_3^+	$^2A_2$	C_{3v} see **1** in Figure 4			−4202.954 52				
	$^2B_2$	C_{2v} see **2** in Figure 4			−4202.948 20				
	$^4A/^4E^i$	C_{3v} see **1** in Figure 4			−4202.865 29[g]				
	$^4B_2$	C_{2v} see **2** in Figure 4			−4202.856 54[g]				
O	^3P				−75.083 02	−74.811 19	−74.863 48	−74.971 45	−75.023 74
O_2	$^3\Sigma_g^-$				−150.357 90	−149.760 26	−149.864 52	−150.124 24	−150.228 50

[a] 1 hartree = 627.51 kcal/mol. [b] B3LYP geometries; similar results were obtained at the other levels of theory, see computational details. [c] Distances in Å and angles in deg. [d] Other states at this level: $^4\Pi = -4118.320\ 61$, $^4\Sigma^+ = -4118.240\ 73$. [e] This energy is for vertical excitation from the quartet state. [f] Other states at this level: $^2B_1 = -4193.418\ 33$, $^2B_2 = -4193.551\ 12$, $^2A_2 = -4193.497\ 81$. [g] These energies are for vertical excitation from the corresponding doublet states. [h] Other states at this level: $^4A_1 = -4193.440\ 94$, $^4B_1 = -4193.440\ 12$, $^4B_2 = -4193.426\ 52$. [i] Because GAUSSIAN92/DFT can only calculate in Abelian point groups, no symmetry could be assigned to the wave function for this C_{3v} structure.

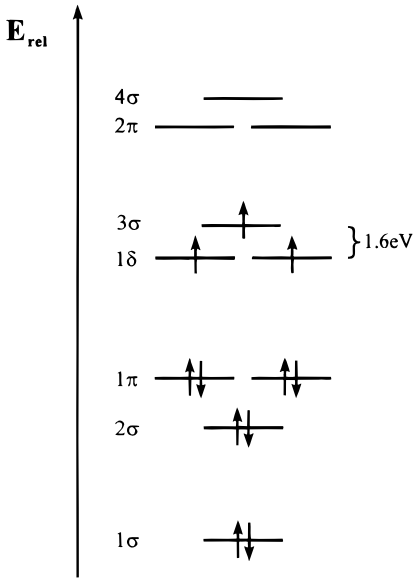

Figure 1. Qualitative molecular orbital scheme for MoO^+ ($^4\Sigma^-$); the energy axis is not calibrated.

be excluded, because MoO^+ ($^6\Sigma^-$) is much less stable than MoO^+ ($^4\Sigma^-$) at all levels of theory applied.

The bonding situation in MoO^+ can be understood in terms of its molecular orbital scheme (Figure 1).[35] The valence orbitals can be divided into bonding (1σ, 2σ, 1π), nonbonding (1δ, 3σ), and antibonding (2π, 4σ) blocks. In MoO^+ ($^4\Sigma^-$), all orbitals of the bonding block are doubly occupied and the unpaired electrons remain in the three nonbonding orbitals in a high-spin situation, suggesting a triple bond between Mo and O. Conceptually, for MoO^+ ($^4\Sigma^-$) a triple bond between Mo and O can be rationalized by formation of a σ bond via donation of the lone pair of oxygen ($2p_\sigma$) into the bonding 5s orbital of molybdenum and overlap of the $4d_\pi$ orbitals of molybdenum with the $2p_\pi$ orbitals of oxygen forming two perpendicular π bonds. However, this description of the $^4\Sigma^-$ state suffers from instabilities that considerably weaken the Mo^+-O bond; i.e. donation of the electrons from the electronegative oxygen to the metal center is not favored. Another possible binding mechanism involves oxygen (^3P) interacting with the first excited state of molybdenum cation Mo^+ (^6D). Here, the singly occupied 5s (Mo) and $2p_\sigma$ (O) orbitals form a strong σ bond, one π bond is realized by overlap of a $4d_\pi$ and a $2p_\pi$ orbital, and the second π bond results from donation of the lone pair of oxygen ($2p_\pi^2$) to the unoccupied $4d_\pi$ orbital of molybdenum cation (^6D). In the latter bonding mechanism a strong σ bond is formed, thus leading to a stabilization of the Mo^+-O bond, but excitation of one electron from a $4d_\pi$ to the 5s orbital renders the triple bond formation energetically unfavorable. Neutral MoO ($^5\Pi$) has been discussed in similar terms by Siegbahn,[36b] who pointed out that the singly occupied $4d_\pi$ orbital in neutral MoO strongly reduces the ability of the metal to accept electrons from the oxygen lone pairs. Following these arguments, one should expect a significant strengthening of the Mo−O interaction upon ionization because precisely the $4d_\pi$ electron is removed, i.e. MoO ($^5\Pi$) → MoO^+ ($^4\Sigma^-$). Nevertheless, BDE(Mo^+-O) is even smaller than that of the neutral (118 versus 133 kcal/mol). Therefore, the bond-order formalism seems to be oversimplified for the description of MoO and MoO^+, and the ionic character of the bonding as well as the corresponding exit channels should also be considered.[29,36a] The real situation is best described by a mixture of the two extreme cases discussed above. Using the MO scheme (Figure 1) and bonding mechanisms for MoO^+, we can explain the large energy gap of 14.1 kcal/mol between the two quartet states MoO^+ ($^4\Sigma^-$) and MoO^+ ($^4\Pi$) with respect to the much smaller difference (2 kcal/mol) in the case of the lower congener CrO^+.[34] In the $^4\Pi$ state of MoO^+ the nonbonding 1δ orbitals are again singly occupied in the same way as in the $^4\Sigma^-$ state, but the third single electron occupies one of the antibonding 2π orbitals. Due to the fact that the 4d orbitals of molybdenum are larger than the corresponding 3d orbitals of chromium, the overlap with the 2p orbitals of oxygen is better for Mo, resulting in an increased $^4\Sigma^-/^4\Pi$ splitting in MoO^+ as compared to CrO^+; i.e. occupation of the antibonding 2π orbital in MoO^+ ($^4\Pi$) is less favorable than that of the 3σ orbital in MoO^+ ($^4\Sigma^-$). The significant energy gap between the 1δ and 3σ orbitals (Figure 1) can almost compensate for the exchange energy loss upon spin coupling, thereby rationalizing the low-lying MoO^+ ($^4\Sigma^-$) → MoO^+ ($^2\Delta$) excitation. Formally, MoO^+ ($^2\Delta$) involves a spin-pairing of the electron in the nonbonding 3σ orbital with one electron in the two singly occupied 1δ orbitals. However, the relativistic stabilization of the 5s orbital that lowers 3σ but not 1δ enlarges the $^4\Sigma^-/^2\Delta$ splitting in favor of the high-spin state.

The BDEs(Mo^+-O) obtained with CAS and CASPT2D are significantly lower than the experimental figure (Table 2); also note the underestimation of BDE(O−O). Although the computed BDEs may approach the experimental ones upon extension of the basis sets[37] as well as the electron correlation treatment, this was not attempted in order to allow for a comparable but still economic theoretical treatment of the other MoX_n^+ species

TABLE 2: Experimental Brackets and Calculated Bond Dissociation Energies (kcal/mol) of MoO_n^+ ($n = 1-3$)[a]

	exptl	B3LYP	B3LYPrel	CAS	CASrel	CASPT2D	CASPT2Drel
Mo^+-O	118 ± 2	99.9	118.9	75.3	94.3	87.1	106.1
OMo^+-O	131 ± 5	123.8	124.5	98.3	99.0	120.1	120.8
O_2Mo^+-O	62 ± 17	75.0					
$O-O$	119.2	120.4	120.2	86.5	86.3	113.8	113.6

[a] The BDEs are calculated with respect to the ground states at the CASPT2Drel level of theory, i.e. $Mo^+(^6S)$, MoO^+ ($^4\Sigma^-$), MoO_2^+ ($^2A_1$), MoO_3^+ ($^2A_2$), and O (^3P).

at the CASPT2D level of theory. As mentioned above, relativity is an important factor affecting BDE(Mo^+-O). In fact, the relativistic correction for BDE(Mo^+-O) amounts to 19 kcal/mol; note that spin−orbit coupling may also be significant but is not considered in this study. The magnitude of this effect can be rationalized by inspection of the singly occupied orbitals in MoO^+ ($^4\Sigma^-$): The two 1δ orbitals do not find a symmetry match on oxygen and thereby remain purely nonbonding. The singly occupied 3σ orbital has slightly antibonding character and is formed from the 5s orbital of molybdenum and the $2p_\sigma$ orbital of oxygen. To a first approximation, relativity has the following effects: (i) radial contraction and energetic stabilization of the s and p shells and (ii) radial expansion and energetic destabilization of the (outer) d and f shells.[20] As a consequence, the relativistic corrections are similar for the 4d orbitals of Mo^+ and the nonbonding 1δ orbitals in MoO^+ and almost compensate each other. Due to its s-character the singly occupied 3σ orbital in MoO^+ ($^4\Sigma^-$) is stabilized by relativity while the 5s orbital is unoccupied in Mo^+ (^6S), resulting in a significant relativistic strengthening of the Mo^+-O bond. In summary, CASPT2Drel predicts BDE(Mo^+-O) = 106.1 kcal/mol, which is by about 10% lower than the experimental figure, mainly due to incompleteness of the one-particle space, while the BDE(Mo^+-O) of 118.9 kcal/mol obtained with the B3LYPrel is close to the experimental figure, though a slight overestimation of the BDE using DFT methods[38] together with fortuitous error compensation can be assumed.[37]

In analogy to the $^4\Sigma^-$ ground state of MoO^+, theory predicts a doublet ground state for MoO_2^+ that is formally derived from spin-pairing between Mo^+ (^6S) and two O (^3P) atoms.[14b,39] The electronic ground state of molybdenum-dioxide cation corresponds to MoO_2^+ ($^2A_1$), while the $^2B_2$ state is only 4.6 kcal/mol less stable at CASPT2Drel and even 0.4 kcal/mol more stable without relativistic correction. Single-point calculations of the quartet states at the B3LYP optimized geometry of the $^2A_1$ state and at the CASPT2D level of theory leads to a very high excitation energy (>50 kcal/mol, see Table 1); thus, these states can be excluded as possible ground states.

For the description of the bonding situation in molybdenum dioxide the contour maps for MoO_2^+ ($^2A_1$) as derived from the CAS calculations are shown in Figure 2. Qualitative analysis of these plots leads to the following orbital descriptions: (i) two almost degenerate doubly occupied, σ-like orbitals ($1a_1$ and $1b_1$, Figure 2a,b) resulting from the interaction of the $4d_z^2$ orbital of Mo with the $2p_x$ orbitals of oxygen and of the $4d_{xz}$ orbital with two $2p_z$ orbitals, respectively; (ii) one doubly occupied σ-like orbital ($2a_1$, Figure 2c) arising from the overlap of the $4d_{x^2-y^2}$ of Mo and two $2p_z$ orbitals at each oxygen atom along with some contributions of 5s (Mo); (iii) two doubly occupied π-like orbitals ($1a_2$ and $1b_2$, Figure 2d,e), which involve the $2p_y$ orbitals on oxygen, which are perpendicular to the plane of the molecule and the $4d_{xy}$ and $4d_{yz}$ orbitals on molybdenum, respectively; (iv) one doubly occupied orbital that is constructed from two $2p_x$ orbitals and has largely nonbonding character ($2b_1$, Figure 2f), because the coefficients on molybdenum are very small (the residual on Mo is mainly due to contributions of the $4p_z$ subshell); finally, (v) the highest singly occupied orbital has σ character ($3a_1$, Figure 2g) and is derived from $4d_{x^2-y^2}$ of Mo (with contributions of 5s) and the two $2p_z$ of O; the $3a_1$ orbital represents the antibonding counterpart of the $2a_1$ orbital. Then, within the valence space several empty orbitals follow: first, $3b_1$ (Figure 2h), which is the antibonding equivalent of $1b_1$ and comprises $4d_{xz}$ and the two $2p_z$ orbitals. Next is $4a_1$ ($4d_{z^2} + 2\cdot2p_x$, Figure 2i), which represents the antibonding equivalent of $1a_1$, and then $5a_1$ (Figure 2j), which by and large represents the empty 5s orbital on Mo. The valence space is completed by the two antibonding counterparts of the $1a_2$ and $1b_2$ orbitals, i.e. $2b_2$ and $2a_2$ (Figure 2k,l) which arise form the combination of $4d_{xy}$ and $4d_{yz}$ with the two $2p_y$ orbitals, respectively. Consideration of these orbitals reveals that MoO_2^+ can be considered as a very stable species, because almost all electrons are located in strongly bonding orbitals. Destabilization is only caused by the two, mainly nonbonding electrons in the $2b_1$ orbital and the singly occupied, slightly antibonding $3a_1$ orbital. Thus, we can classify the bonding in MoO_2^+ ($^2A_1$) as that of two metal oxygen double bonds and assign a formal oxidation state of +V to molybdenum.

Irrespective of the level of theory applied, the computations predict that BDE(OMo^+-O) exceeds BDE(Mo^+-O) by ca. 10 kcal/mol, and the stability difference amounts to 14.7 kcal/mol at CASPT2Drel (Table 2). At first sight, this result seems unexpected because one may argue that an increase of the formal oxidation state of the metal would lower the BDE. In fact, the arguments raised above demonstrate that the increase of the BDE going from MoO^+ to MoO_2^+ is due to the high stability of MoO_2^+ and vice versa by the destabilizing factors in MoO^+. Another factor explaining the high BDE in OMo^+-O is that the very stable half-filled $4d^5$ configuration at the Mo^+ center is broken upon addition of the first oxygen ligand. This is no longer the case for addition of the second oxygen ligand; thus BDE(OMo^+-O) > BDE(Mo^+-O). Note that analogous differences have been described by Siegbahn for the neutral molybdenum oxides and a similar explanation has been put forward.[36b]

An aspect that deserves further discussion is relativity, which largely differs for molybdenum mono- and dioxides. While in MoO^+ the relativistic correction to the BDE amounts to almost 20 kcal/mol, the relativistic effect on the BDE(OMo^+-O) is negligible (0.7 kcal/mol). This pronounced difference can be explained by inspection of the population analysis (Table 3): As mentioned, relativity stabilizes the s and p orbitals while destabilizing d and f orbitals. In fact, the population of the 5s orbital in the metal dioxide MoO_2^+ ($^2A_1$) amounts to only about one-third of that in MoO^+ ($^4\Sigma^-$). As a consequence, the MoO^+ molecule experiences a significant relativistic stabilization, while relativity affects MoO_2^+ to a much lesser extent.

The calculations of MoO_3^+ were performed only at the B3LYP level of theory due to computational restrictions. According to these results, the ground state of MoO_3^+ arises from the doublet surface and exhibits the C_{3v}-symmetrical structure **1** (Figure 3). The planar, C_{2v}-symmetrical structure **2** is 4 kcal/mol higher in energy and corresponds to a transition structure (TS) for a degenerate rearrangement of **1**. The quartet states were not further investigated, because these are very high

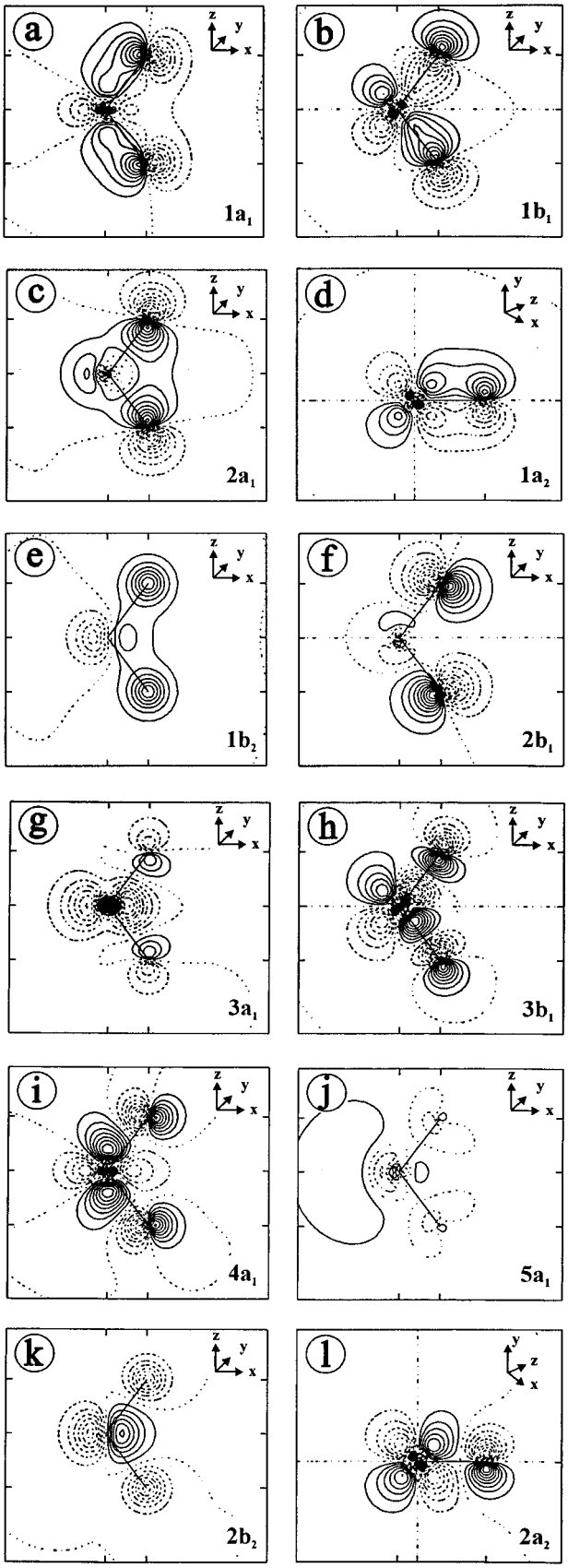

Figure 2. Contour diagrams of the atomic natural orbitals of MoO_2^+ ($^2A_1$) as derived from the CAS calculations. Plots d and l are shown along one of the Mo−O bonds. Plots e and k have an offset of +0.33 a_0 along the *z*-axis.

in energy for **1** as well as **2**. At the B3LYP level of theory, the calculated BDE(O_2Mo^+−O) amounts to 75 kcal/mol. Irrespective of the tendency for a slight overbinding with DFT,[38] this figure is in accord with the rough experimental bracket of 62 ± 17 kcal/mol. Due to the failure to perform CASSCF and CASPT2D calculations, a further evaluation of this figure as well as relativistic corrections are impossible for the time being. Nevertheless, relativity is expected to be of minor importance for MoO_3^+ ($^2A_2$) because the 5s occupancy is even lower than in MoO_2^+ ($^2A_1$) for which ΔBDE_{rel} is negligible (Table 3). The bonding situation in MoO_3^+ ($^2A_2$) can best be described by attachment of an additional oxygen atom O (^3P) to the MoO_2^+ ($^2A_1$) ground state. However, in **1** all Mo−O bonds are identical, indicating a stabilization by mesomeric resonance. Structure **1** is very similar to that of the corresponding neutral MoO_3 (r_{Mo-O} = 1.70 Å, C_{3v} symmetry),[36b] which contains a high-valent Mo(VI) oxidation state. This bonding picture also rationalizes the rather large ionization energy of MoO_3 (11.7 eV), because ionization must involve the highest molecular orbital, e.g. a lone pair at oxygen or a Mo−O π bond; in fact, similar IEs are found for other transition-metals in their highest oxidation states,[25] e.g. IE(CrO_3) = 11.6 eV, IE(WO_3) = 12.5 eV, IE(CH_3ReO_3) = 10.2 eV,[40] IE(RuO_4) = 12.2 eV, and IE(OsO_4) = 12.3 eV.

TABLE 3: Natural Bond Orbital (NBO) Populations at the B3LYP Level of Theory for Partical Charges and Occupancies of 4d and 5s Orbitals at Molybdenum in MoX_n^+ Cations (X = O, S; *n* = 1−3) Together with the Relativistic Bond Strengthening (ΔBDE_{rel}) Derived from the CAS Calculations

	state	Mo(*q*)	4d	5s	ΔBDE_{rel}
MoO^+	$^4\Sigma^-$	+1.34	4.06	0.60	19.0
MoO_2^+	$^2A_1$	+1.72	4.12	0.16	0.7
MoO_3^+	$^2A_2$	+1.86	4.04	0.1	
MoS^+	$^4\Sigma^-$	+0.90	4.68	0.42	13.5
MoS_2^+	$^2A_1$	+0.69	5.02	0.29	3.5
MoS_3^+	$^2A_2$	+0.37[a]	5.32	0.31	
	$^4A''$	+0.88[b]	4.93	0.19	

[a] Corresponding to structure **6** in Figure 5. [b] Corresponding to structure **8** in Figure 5.

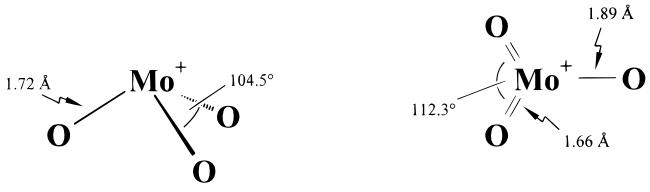

Figure 3. Geometries of the trioxides MoO_3^+ ($^2A_2$) and MoO_3^+ ($^2B_2$) calculated at the B3LYP level of theory (bond lengths in Å and angles in deg).

Reactivity of MoO_n^+ Cations. Before addressing the reactions of MoO_n^+ with hydrocarbons, we wish to apply the knowledge of the electronic ground states for *n* = 1−3 in order to obtain further insight into the reaction of MoO_n^+ cations (*n* = 0−2) with dinitrogen oxide. From a thermochemical point of view, N_2O seems to be the reactant of choice for converting metal cations into their oxides. This is due to the high stability of the N_2 molecule, which renders oxygen-atom transfer rather exothermic for many elements, i.e. BDE(NN−O) = 40 kcal/mol. Under FTICR conditions the rate constants of the oxidation reactions 7−9 do, however, not correlate with the associated reaction exothermicities.

$$Mo^+ + N_2O \rightarrow MoO^+ + N_2$$
$$k \leq 6.0 \times 10^{-13}\ cm^{-3}\ s^{-1}\ molecule^{-1}$$
$$\Delta_R H° = -78 \pm 2\ kcal/mol \quad (7)$$

$$MoO^+ + N_2O \rightarrow MoO_2^+ + N_2$$
$$k = 5.6 \times 10^{-10}\ cm^{-3}\ s^{-1}\ molecule^{-1}$$
$$\Delta_R H^\circ = -87 \pm 4\ kcal/mol \quad (8)$$

$$MoO_2^+ + N_2O \rightarrow MoO_3^+ + N_2$$
$$k = 3.7 \times 10^{-10}\ cm^{-3}\ s^{-1}\ molecule^{-1}$$
$$\Delta_R H^\circ = -26 \pm 6\ kcal/mol \quad (9)$$

In view of the substantial thermodynamic driving forces, considerable kinetic barriers must be operative, in particular in reaction 7. Inspection of the computational results discussed above reveals that the multiplicity changes from 6 to 4 in reaction 7 and from 4 to 2 in reaction 8, but remains constant at 2 in the oxidation of MoO_2^+ to MoO_3^+. As already discussed in the literature,[41] we suggest a simple rationale for the different rate constants for reactions 7−9 based on spin conservation arguments. First, the exothermicities quoted above only apply if the corresponding ground states of the oxides are formed during the reaction. Because N_2O as well as N_2 are singlets, spin−orbit coupling must mediate curve crossings in reactions 7 and 8 in order to allow for the necessary changes in spin multiplicity. Second, the complexation energy of N_2O to metal cations is not very large,[42,43] because the anisotropy and the polarizability of the N_2O molecule are small. As a consequence the cross sections and the probabilities for the occurrence of reactions 7−9 will only be high if the reactions are exothermic for the corresponding ground states and adequate excited states, respectively, or if the curve crossing to the lower spin surface occurs very early. Thus, if reaction 7 proceeded with spin conservation it would initially involve the highly excited MoO^+ ($^6\Sigma^-$) state and hence be endothermic. As a consequence, curve crossing to the quartet surface must occur in the vicinity of the putative transition structure for O-atom transfer such that the reaction is therefore very inefficient (Figure 4). A different situation is found for reaction 8 because the quartet state of MoO_2^+ ($^4A_2$) is not too energy demanding with regard to the overall reaction exothermicity, the spin-conserving reaction pathway is feasible, and curve crossing to the low-spin dioxide can occur in the exit channel. Lastly, reaction 9 is not subject to any spin constraints and indeed takes place relatively efficiently despite having the lowest exothermicity of reactions 7−9.

The reactivity of MoO_n^+ ($n = 0-2$) toward small hydrocarbons, such as methane and ethane, has been studied by Cassady and McElvany,[7] and their major observations were: (i) single and double dehydrogenations dominate in the reactions of Mo^+ and MoO^+, while the dioxide MoO_2^+ exhibits a preference for C−C bond activation as well as loss of neutral water, (ii) addition of oxygen ligands to Mo^+ increases the reaction rates as compared to the bare metal cation, in line with a disruption of the inert d^5 system of Mo^+ (^6S), and (iii) finally, from the occurrence and nonoccurrence of secondary reactions it was concluded that the number of available coordination sites on molybdenum is the major cause for differences in reactivity. So as to check the comparability of our results, we repeated the reaction of MoO_2^+ with ethane, and our results concur with those of Cassady and McElvany within experimental error.[44] Therefore, the results reported in ref 7 for the reactions of MoO^+ and MoO_2^+ with methane and ethane were adopted.

Inspection of Table 4 reveals that MoO_3^+ has a much higher reactivity than the lower molybdenum oxides. In particular, MoO^+ and MoO_2^+ cannot activate methane, whereas MoO_3^+ reacts quite rapidly. This trend continues for the other substrates and abstraction of hydrogen atoms and electron transfer are the major reaction pathways observed for MoO_3^+; further, MoO_3^+ even abstracts a hydrogen atom from water, and thus BDE(MoO_3^+−H) > 118 kcal/mol. In contrast, the lower oxides MoO^+ and MoO_2^+ mainly undergo dehydrogenation and dehydration reactions, respectively, with alkanes, and C−H bond activation also prevails in the reactions of these oxides with arenes.

Activation of methane by MoO_3^+ can be explained by the mechanisms depicted in Scheme 1. Thus, we propose that initially the cation radical of the high-valent transition-metal oxide abstracts a hydrogen atom from methane to form a loose

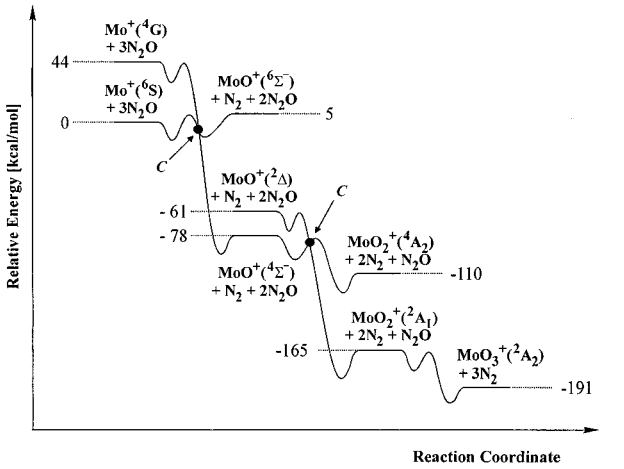

Figure 4. Schematic potential-energy surface for the reaction of Mo^+ with N_2O; the letter *C* denotes a curve crossing between the different spin multiplicities. For the sake of clarity, we omitted the crossing with the excited state of N_2O, which is analyzed in detail elsewhere; see ref 41a.

TABLE 4: Branching Ratios and Rate Constants in $cm^3\ s^{-1}$ $molecule^{-1}$ for the Reactions of MoO_n^+ ($n = 1-3$) with Selected Hydrocarbons

reactant	neutral product	MoO^+	MoO_2^+	MoO_3^+
methane	$CH_3^\bullet$			75
	H_2O	no reaction		4
	CH_2O			20
	CH_4O			1
	k_{exp}	$<10^{-13}$ [a]	$<10^{-13}$ [a]	7×10^{-10}
ethane	H_2	95[a]		
	$2H_2$	5[a]		
	H_2O		100[a]	
	MoO_3H			40
	$C_2H_5^\bullet$			20
	C_2H_4			40
	k_{exp}	6.7×10^{-10} [a]	2.3×10^{-10} [a]	15.4×10^{-10}
benzene	H_2	70		
	H_2O		50	10
	CO	15	15	
	$C_6H_5^\bullet$			40
	C_6H_6O			5
	MoO_3 (ET)			35
	MoO_3H			10
	adduct[b]	20	35	
	k_{exp}	6.6×10^{-10} [a]	9.9×10^{-10}	16.2×10^{-10}
toluene	$H^\bullet$	50		
	$OH^\bullet$		4	
	MoO_n (ET)		1	80
	H_2	50		
	H_2O		55	
	MoO_nH		30	20
	adduct[b]		10	
	k_{exp}	16.0×10^{-10}	9.4×10^{-10}	18.1×10^{-10}

[a] Values taken from ref 7 and fully confirmed in our laboratories, see ref 44. [b] This entry denotes the association of other reactants to yield the corresponding adduct complexes.

TABLE 5: Branching Ratios for the Reactions of MoO_3^+ with Deuterated Methanes $CH_{4-n}D_n$ (n = 0, 2, 4)[a]

	n	$\sim H^\bullet$	$\sim D^\bullet$	$-H_2O$	$-HDO$	$-D_2O$	$-CH_2O$	$-CHDO$	$-CD_2O$	$-[CH_{4-n}D_nO]$[b]
CH_4	0	75		4			20			1
CH_2D_2	2	50	22	4	4	<1	1	12	6	1
CD_4	4		86			5			8	1

[a] $\sim H^\bullet$ and $\sim D^\bullet$ denote homolytic C−H/C−D bond cleavages by MoO_3^+ leading to MoO_3H^+ and MoO_3D^+, respectively. [b] In the thermochemical considerations the neutral $[CH_mD_nO]$ is assumed to correspond to methanol. The position of the deuterium label in the neutral product cannot be assessed in the experiment.

SCHEME 1

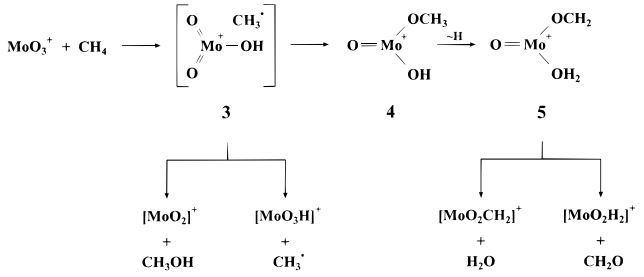

complex **3**, which can either directly dissociate into MoO_3H^+ and $CH_3^\bullet$ or collapse to the intermediate **4**, followed by rearrangement to **5**. The latter ions can then account for the losses of neutral water and formaldehyde, respectively. Note that the formation of MoO_2^+ concomitant with CH_3OH formation was used to derive the upper limit of $BDE(O_2Mo^+-O) < 90$ kcal/mol. Isotopic labeling (Table 5) shows that the C−H versus C−D bond activation of [D_2]methane by MoO_3^+ to yield MoO_3H^+ and MoO_3D^+, respectively, is associated with a kinetic isotope effect of $k_H/k_D \approx 2$. In addition, analysis of the minor reaction products suggests the operation of an isotope effect in the formation of **4** and **5**. Further, upon complete deuteration of methane the yield of MoO_3D^+ increases, most likely due to hindrance of the subsequent rearrangements by the operation of kinetic isotope effects. In the reaction of MoO_3^+ with ethane, single and double hydrogen-atom abstractions occur, as well as ET from the initially formed ethyl radical to MoO_3H^+, to yield the neutral hydroxide and ethyl cation. Similarly, C−H bond activation occurs with the arenes, and, due to the low IEs of benzene and toluene, ET to produce neutral MoO_3 is intense. In summary, the reactions of MoO_3^+ can be considered as typical processes of a radical cation, i.e. atom abstraction and electron transfer; O-atom transfer from the metal oxide to the substrate is limited to a few side reactions.[45]

Molybdenum Sulfide Cations MoS^+, MoS_2^+, and MoS_3^+. *Generation and Thermochemistry of Molybdenum Sulfide Cations*. In 1981, Freiser and co-workers[46] demonstrated that ethylene sulfide allows sequential S-atom transfer to transition-metal ions. However, we found that this reagent is not ideal for the study of subsequent ion/molecule reactions because several side reactions take place, and moreover, the reagent cannot readily be pumped away when introduced via pulsed valves. Therefore, carbonyl sulfide was used as a sulfur donor that exhibits good pumping properties and reacts at reasonably high rates. Sequential sulfur transfer continues up to MoS_5^+ as the final product that does not react further with COS.

$$Mo^+ + COS \rightarrow MoS^+ + CO \qquad k = 2.6 \times 10^{-10}\ cm^{-3}\ s^{-1}\ molecule^{-1} \quad (10)$$

$$MoS^+ + COS \rightarrow MoS_2^+ + CO \qquad k = 5.8 \times 10^{-10}\ cm^{-3}\ s^{-1}\ molecule^{-1} \quad (11)$$

$$MoS_2^+ + COS \rightarrow MoS_3^+ + CO \qquad k = 2.9 \times 10^{-10}\ cm^{-3}\ s^{-1}\ molecule^{-1} \quad (12)$$

$$MoS_3^+ + COS \rightarrow MoS_4^+ + CO \qquad k = 8.2 \times 10^{-10}\ cm^{-3}\ s^{-1}\ molecule^{-1} \quad (13)$$

$$MoS_4^+ + COS \rightarrow MoS_5^+ + CO \qquad k = 0.6 \times 10^{-10}\ cm^{-3}\ s^{-1}\ molecule^{-1} \quad (14)$$

From the occurrence of reactions 10−14 we can derive lower limits of $BDE(S_nMo^+-S) \geq 72$ kcal/mol (n = 0−4), and unlike the O-atom transfer from N_2O, spin constraints do not seem to play crucial roles. However, no further insight can be gained from these reactions, and therefore, we examined sequential sulfur transfer to molybdenum cation using CS_2 as the transferring reagent.

$$Mo^+ + CS_2 \rightarrow MoS^+ + CS \qquad k \approx 0.7 \times 10^{-12}\ cm^{-3}\ s^{-1}\ molecule^{-1} \quad (15)$$

$$MoS^+ + CS_2 \rightarrow MoS_2^+ + CS \qquad k = 3.3 \times 10^{-11}\ cm^{-3}\ s^{-1}\ molecule^{-1} \quad (16)$$

$$MoS_2^+ + CS_2 \not\rightarrow MoS_3^+ + CS \qquad k < 10^{-13}\ cm^{-3}\ s^{-1}\ molecule^{-1} \quad (17)$$

The formation of MoS_n^+ (n = 1, 2) in reactions 15 and 16 suggests lower limits of $BDE(S_nMo^+-S) \geq 102$ kcal/mol for n = 0, 1. However, the rather low rate constant of reaction 15, i.e. $k_{exp}/k_{ADO} < 0.001$, led us to the suspicion that MoS^+ may evolve from impurities in the carbon disulfide used. Although we carefully purified this reagent,[47] contamination of CS_2 by carbonyl sulfide in the subpercent range cannot be excluded, and in fact the apparent rate constant of reaction 15 is larger for a crude sample of CS_2. Thus, we suspect that the observation of reaction 15 is due to an impurity. The subsequent reaction 16 is considerably more efficient and must at least in part arise from CS_2 rather than COS, because otherwise the measured rate constants of reactions 15 and 16 would correlate with those of reactions 10 and 11. Anyhow, reaction 16 is still slow, and to a very first approximation we, again, neglect any activation barrier for sulfur-atom transfer and apply the Arrhenius formalism (see above), which suggests $BDE(SMo^+-S) = 100 \pm 14$ kcal/mol using a rather conservative error estimate. The apparent failure to observe reactions 15 and 17 leads to brackets of 72 kcal/mol ≤ $BDE(S_nMo^+-S) \leq 102$ kcal/mol (n = 0, 2), or $BDE(Mo^+-S) = 88 \pm 14$ kcal/mol and $BDE(S_2Mo^+-S) = 88 \pm 14$ kcal/mol; the use of the nonoccurrence of reactions 15 and 17 to derive upper limits seems to be justified, because in the analogous reactions of COS no substantial barriers are apparent. Using the same methodology as for the molybdenum oxides, the ionization energies of the sulfides were determined as $IE(MoS) = 7.7 \pm 0.3$ eV, $IE(MoS_2) = 8.6 \pm 0.3$ eV, and $IE(MoS_3) = 8.9 \pm 0.3$ eV, respectively. Unfortunately, these

TABLE 6: Geometries and Total Energies (hartree)[a] of Different Electronic States of MoS_n^+ ($n = 0-3$)

	state	geometry[b,c]			B3LYP	CAS	CASrel	CASPT2D	CASPT2Drel
		r_{Mo-S}	r_{Mo-S}	α_{S-Mo-S}					
Mo^+	^6S				−3977.229 37	−3975.238 35	−4042.873 89	−3975.513 90	−4043.149 44
MoS^+	$^2\Delta$	2.04			−4375.417 35	−4372.769 05	−4441.497 60	−4373.236 24	−4441.964 79
	$^4\Sigma^-$	2.08			−4375.445 67	−4372.811 43	−4441.548 35	−4373.279 43	−4442.016 35[d]
	$^6\Sigma^-$	2.08			−4375.367 17[e]	−4372.736 27	−4441.470 30	−4373.221 48	−4441.955 51
MoS_2^+	$^2A_1$	2.09	2.09	105.5	−4773.685 47	−4770.417 17	−4840.239 52	−4771.072 33	−4840.894 68[f]
	$^4A_2$	2.09	2.09	105.5	−4473.646 05	−4770.363 11	−4840.184 11	−4771.032 25	−4840.853 25[g]
MoS_3^+	$^2A_2$	C_{3v} see **6** in Figure 5			−5171.911 95				
	$^2A_2'$	D_{3h} see **7** in Figure 5			−5171.879 13				
	$^4A/^4E^h$	C_{3v} see **6** in Figure 5			−5171.862 31[i]				
	$^4A''$	C_s see **8** in Figure 5			−5171.887 51				
S	^3P				−398.103 12	−397.504 79	−398.584 57	−397.660 18	−398.739 96
S_2	$^3\Sigma_g^-$				−796.361 97	−795.126 35	−797.285 31	−795.467 19	−797.626 15

[a] 1 hartree = 627.51 kcal/mol. [b] B3LYP geometries; similar results were obtained at other levels of theory, see computational details. [c] Distances in Å and angles in deg. [d] Other states at this level: $^4\Pi = -4441.981\ 13$, $^4\Sigma^+ = -4441.909\ 62$. [e] This energy was derived by vertical excitation from the quartet to the doublet surface. [f] Other states at this level: $^2B_1 = -4840.817\ 51$, $^2B_2 = -4840.859\ 58$, $^2A_2 = -4840.856\ 12$. [g] Other states at this level: $^4A_1 = -4840.831\ 81$, $^4B_1 = -4840.838\ 59$, $^4B_2 = -4840.822\ 37$. [h] Because GAUSSIAN92/DFT can only calculate in Abelian point groups, no symmetry could be assigned to the wave function for this C_{3v} structure. [i] This energy is for vertical excitation from the doublet state.

TABLE 7: Experimental Brackets and Calculated Bond Dissociation Energies (kcal/mol) of MoS_n^+ ($n = 1-3$) at Different Levels of Theory[a]

	exptl	B3LYP	B3LYPrel	CAS	CASrel	CASPT2D	CASPT2Drel
Mo^+-S	88 ± 14	71.0	84.5	42.9	56.4	66.1	79.6
SMo^+-S	100 ± 14	85.8	89.3	63.4	66.9	83.3	86.8
S_2Mo^+-S	88 ± 14	77.4					
S−S	102	97.7	97.3	73.3	72.9	92.1	91.7

[a] The BDEs are calculated with respect to the ground states at the CASPT2Drel level of theory, i.e. Mo^+ (^6S), MoS^+ ($^4\Sigma^-$), MoS_2^+ ($^2A_1$), MoS_3^+ ($^2A_2$), and S (^3P).

data cannot be used for a refinement of the BDEs, because we are not aware of gas-phase thermochemistry data for neutral MoS_n ($n = 1-3$). While the thermochemistry derived in these experiments is in reasonable agreement with the theoretical figures (see below), the accuracy is poor and a more thorough evaluation of the thermochemistry of the neutral and cationic $MoS_n^{0/+}$ is desirable.

Computational Study of the MoS_n^+ System. The molybdenum-monosulfide cation exhibits the same $^4\Sigma^-$ ground state as MoO^+. In contrast to the close spacing of the $^2\Delta$ and $^4\Sigma^-$ states in the monoxide, these states are well separated for MoS^+, i.e. 18 kcal/mol with B3LYP and 27 kcal/mol at the CAS level of theory, respectively (Table 6). At the CASPT2Drel level of theory MoS^+ ($^4\Sigma^-$) is even 32 kcal/mol more stable than MoS^+ ($^2\Delta$). The sextet MoS^+ ($^6\Sigma^-$) is much higher in energy than the MoS^+ ($^4\Sigma^-$) ground state at all levels of theory applied and was not examined further.

The binding situation in MoS^+ is very similar to that discussed above for MoO^+. A notable difference concerns the energy gap between the 1δ and 3σ orbitals, which decreases from $\Delta E = 1.6$ eV for the oxide to $\Delta E = 0.4$ eV in the sulfide. As a result, the near degeneracy of the $^2\Delta$ and $^4\Sigma^-$ states vanishes for the MoS^+, because Hund's rule can be applied without occupying high-energy orbitals. Similar to MoO^+, relativity is important for MoS^+, though the relativistic bond strengthening ΔBDE_{rel} is slightly reduced following the 5s occupancy (Table 3). The BDEs(Mo^+-S) computed with B3LYPrel and CASPT2Drel agree with the experimental range (Table 7); however, the underestimation of BDE(S−S) at all levels of theory implies that the description is far from being complete.

The calculated properties of MoS_2^+ are also very similar to those of MoO_2^+; i.e. the ground state corresponds to MoS_2^+ ($^2A_1$), and the quartet states are substantially higher in energy, such that we refrain from a detailed discussion of the disulfide. The BDEs(SMo^+-S) computed at various levels of theory are somewhat lower than the experimental figure, but the deviation is within the expected accuracy of this approach. In analogy to the MoO^+/MoO_2^+ couple, the computed BDEs(SMo^+-S) are significantly larger than the BDEs(Mo^+-S) irrespective of the theoretical method applied. The relativistic effects decrease from MoS^+ to MoS_2^+; note that this effect is smaller than for the pair MoO^+/MoO_2^+ completely in line with the smaller difference in 5s occupation between MoS^+ and MoS_2^+ (Table 3).

For MoS_3^+ the results are restricted to those obtained with the B3LYP method, because similar to the trioxide the computational demands are too high even with CASSCF. In accordance with the trioxide, MoS_3^+ exhibits a C_{3v}-symmetrical doublet ground state ($^2A_2$) with structure **6** as shown in Figure 5. Efforts to locate a stationary point similar to the trioxide structure **2** on the doublet surface of MoS_3^+ led to the D_{3h}-symmetrical transition structure **7** lying 20.6 kcal/mol above MoS_3^+ ($^2A_2$). Further, the doublet/quartet splitting for the C_{3v} structure **6** was assessed by vertical excitation from the doublet to the quartet surface and displays that the quartet state with C_{3v} structure lies 31 kcal/mol above MoS_3^+ ($^2A_2$). B3LYP predicts a BDE(S_2-Mo^+-S) of 77.4 kcal/mol, which is in accordance with the experimental value of 88 ± 14 kcal/mol. As far as the effect of relativity is concerned, the similar 5s occupancies in MoS_3^+ ($^2A_2$) and MoS_2^+ ($^2A_1$) suggest a ΔBDE_{rel} on the order of a few kcal/mol also for MoS_3^+ (Table 3).

An interesting aspect of the $[Mo,S_3]^+$ system is that there exists another minimum on the quartet surface MoS_3^+ ($^4A''$), which exhibits the C_S symmetrical structure **8** (Figure 5) and is located only 15 kcal/mol above MoS_3^+ ($^2A_2$). The connectivity of **8** can be understood as binding between Mo^+ and a S_3 moiety, as implied by the short S−S distance (2.11 Å) together with Mo−S distances of 2.34 and 2.41 Å, respectively. Hence, **8** represents a 4d element polysulfide.[46,48] The fact that the high-spin states of transition-metal sulfides, e.g. $^4MoS_3^+$, can exhibit polysulfide structures can be attributed to the electronic situation of the metal center. In the case of Mo^+ (d^5), two of the sulfur

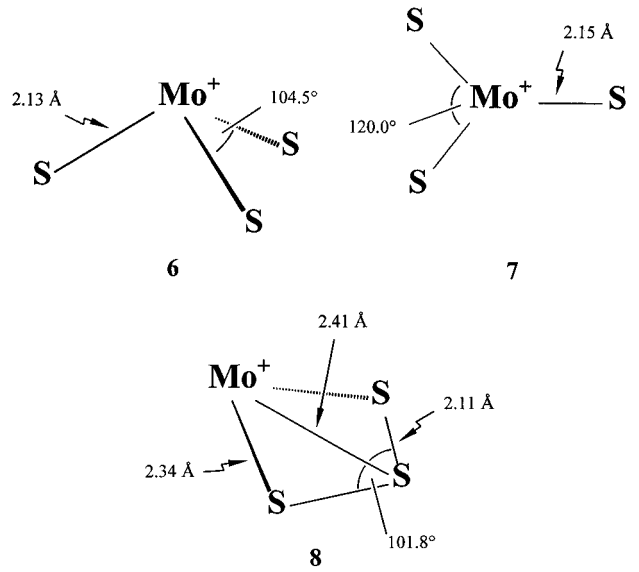

Figure 5. Geometries of the trisulfides MoS_3^+ ($^2A_2$), MoS_3^+ ($^2A_2'$), and MoS_3^+ ($^4A''$) calculated at the B3LYP level of theory (bond lengths in Å and angles in deg).

TABLE 8: Branching Ratios and Rate Constants in $cm^3\ s^{-1}$ $molecule^{-1}$ for the Reactions of MoS_n^+ ($n = 1-3$) with Selected Hydrocarbons

reactant	neutral product	MoS^+	MoS_2^+	MoS_3^+
methane			no reaction	
	k_{exp}	$<10^{-13}$	$<10^{-13}$	$<10^{-13}$
ethane	H_2	100	100	100
	k_{exp}	2.9×10^{-10}	3.0×10^{-10}	3.4×10^{-10}
benzene	H_2	30		no reaction
	adduct[a]	70	100	
	k_{exp}	4.6×10^{-10}	2.6×10^{-10}	$<10^{-12}$
toluene	H_2	100	25	
	MoS_nH		10	90
	MoS_n (ET)		5	10
	adduct[a]		60	
	k_{exp}	10.9×10^{-10}	7.6×10^{-10}	9.5×10^{-10}

[a] This entry denotes the association of other reactants to yield the corresponding adduct complexes.

atoms can form a bond with Mo^+, whereas the third one can either donate its lone pair into the empty 5s orbital or form two single bonds to the other sulfur atoms. In the latter configuration, the sulfur valences are saturated and the four-membered ring in structure **8** is formed as a high-spin state. Most probably, the higher sulfide ions MoS_4^+ and MoS_5^+ that are formed in reactions 13 and 14 also have polysulfide structures. Nevertheless, thermochemical considerations in conjunction with the theoretical results suggest that structure **8** is not involved in the formation of MoS_3^+ via reaction 12.

Reactivity of MoS_n^+ Cations. The reactivity of the MoS_n^+ cations toward hydrocarbons differs entirely from that of the oxides. The only processes observed are C−H bond activation, electron transfer, and adduct formation.

Table 8 reveals that none of the sulfides react with methane and the only process observed with ethane is dehydrogenation. The reactivity with benzene decreases with increase of the number of sulfur ligands. Toluene, which bears aromatic as well as aliphatic hydrogen atoms, readily reacts with MoS^+ under loss of H_2. The disulfide is the least reactive of the three sulfides, as shown by the high percentage of adduct formed with toluene. MoS_3^+ reacts with toluene *via* the same reaction pathways as the trioxide, i.e. electron- and hydrogen transfer, but with an opposite ratio. Thus, while electron transfer is the process of choice for the trioxide, hydrogen transfer is the main for the trisulfide.

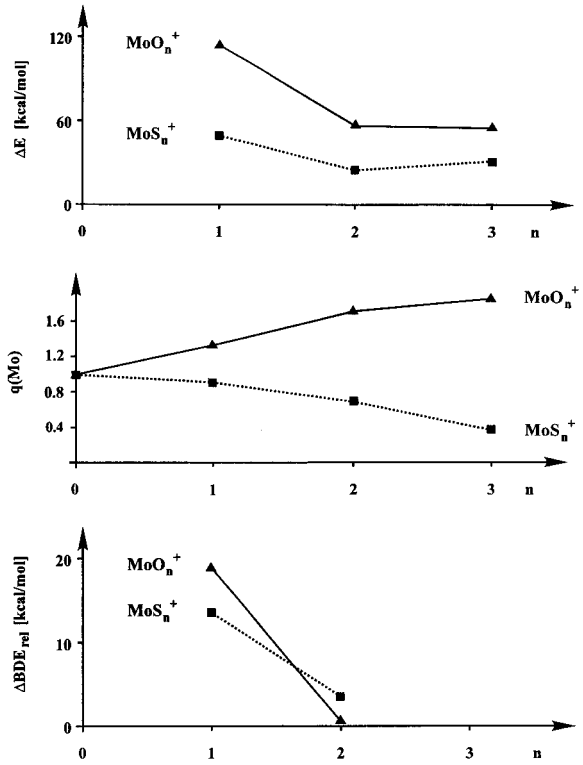

Figure 6. (a, top) High-spin/low-spin splitting (ΔE) for MoX_n^+ cations calculated at the B3LYP level of theory. (b, middle) NBO charges at molybdenum q(Mo) in the MoX_n^+ cations at the B3LYP level of theory. (c, bottom) Relativistic effects (ΔBDE_{rel}) on the $BDE(X_nMo-X)$ ($n = 0, 1$; X = O, S) at the CASrel level of theory. The symbols (▲) and (■) correspond to MoO_n^+ and MoS_n^+, respectively.

Comparison of Cationic Molybdenum Oxides and Sulfides

In this section the molybdenum oxide and sulfide cations are compared with respect to electronic ground states, binding situations, thermochemical properties, and reactivities in order to show similarities and distinct differences in their gas-phase chemistry. In general, metal oxides and sulfides show the same electronic ground states, as expected from the similar valence structures of oxygen and sulfur.[49] Yet, differences in thermochemistry and reactivity arise from the fundamental physical properties (e.g. polarizability and electronegativity) of the chalcogenide ligands.

Electronic States and Binding Situations. The molybdenum-oxide cations and their sulfur counterparts exhibit the same ground states and closely related structural parameters when the longer Mo−S bonds are taken into account.

A more general way to compare oxides and sulfides is provided by the high-spin/low-spin (HS/LS) splittings. Throughout the MoX_n^+ series, the HS/LS splittings are much smaller (ca. 50%) for the sulfides than for the oxides (Figure 6a). This trend can be traced back to the fact that the Mo−O π-bonds are stronger than the Mo−S π-bonds, simply because isovalent hybridization[50] of the 2s and the 2p orbitals of oxygen is favorable as compared to the 3s and 3p orbitals of sulfur. Hence, the $\pi \rightarrow \pi^*$ splitting is smaller for sulfur such that the $\pi \rightarrow \pi^*$ excitation is more facile and the HS/LS splitting is less pronounced. The partial charges at the molybdenum centers (Figure 6b) reflect the different electronegativities of oxygen and sulfur. Thus, oxygen acts as an electron-withdrawing

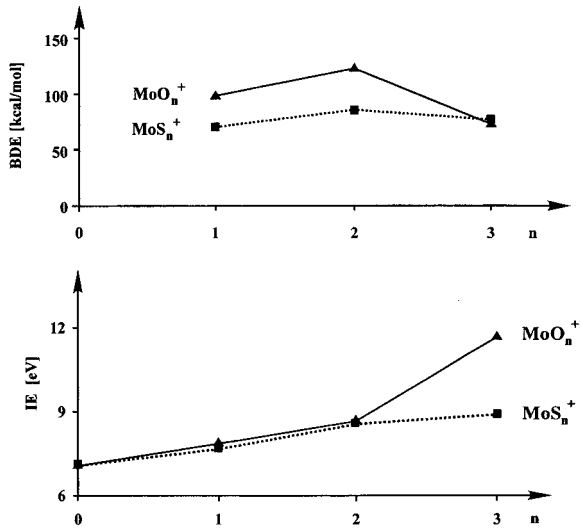

Figure 7. (a, top) Bond dissociation energies (BDE) for oxides and sulfides at the B3LYP level of theory. (b, bottom) Experimental ionization energies (IE) for molybdenum oxides and sulfides. The symbols (▲) and (■) correspond to MoO_n^+ and MoS_n^+, respectively.

ligand, and the positive charge at the molybdenum center increases with the number of oxygen ligands. In contrast, the positive charge at molybdenum decreases along the MoS_n^+ series, due to the electron-donating properties of sulfur such that the charge is more delocalized. The relativistic effects on the BDE (ΔBDE_{rel}) are presented in Figure 6c; for MoX_3^+ no values are available. Comparison of the relativistic effects on the BDE shows that the influence of relativity is pronounced for the first ligand but small, if not negligible, for the second. This alternation can be attributed to the empty 5s orbital in Mo^+ (^{6}D) as compared to the significant 5s occupation in MoX^+, while the second chalcogenide ligand decreases the 5s occupation, thus decreasing ΔBDE_{rel}. However, the difference in ΔBDE_{rel} going from MoX^+ to MoX_2^+ is less pronounced for sulfur than for the electronegative oxygen ligand. Further, the relativistic effects for MoX_n^+ (X = O, S; n = 1, 2) correlate reasonably well with the corresponding 5s occupations (Table 3).

A particular aspect of the bonding situation is revealed by the polysulfide structures found for MoS_3^+, which represent a fundamental difference to the metal oxides for which peroxide formation is much less likely. Polysulfide formation also accounts for the continuing sulfur transfer from COS to MoS_3^+ ending up in the MoS_5^+ cation, and even larger metal sulfides can be made when other reagents, as for example gaseous sulfur,[48] are used.

Thermochemistry. Comparison of the BDEs calculated at the B3LYP level of theory (Figure 7a) reveals an alternation for both MoO_n^+ and MoS_n^+ (n = 1−3): The first chalcogenide ligand is more weakly bonded to the molybdenum than the second, while the $BDE(X_2M^+-X)$ is the smallest. Similar odd/even alternations have been reported for FeS_n^+ (n = 0−6).[46] The small BDE of the first ligand can be attributed to the occupation of slightly antibonding orbitals and destruction of the inert d^5 configuration at Mo^+ as discussed above. Addition of the second ligand is accompanied by perfect pairing of the two nonbonding electrons in MoX^+ ($^4\Sigma^-$) with the two unpaired electrons in O (^{3}P), thus leading to a higher $BDE(XMo^+-X)$. Recalling the binding situation in the trioxide, the reason for the decrease of BDE going from n = 2 to n = 3 becomes obvious. Due to the perfect pairing in the dioxide, only one electron is left at the metal center for the binding of a third chalcogenide ligand, though stabilization *via* mesomeric resonance slightly reduces this effect. The situation is somewhat different when oxygen is replaced by sulfur. In the trisulfide the cationic character of the molybdenum center is much reduced (Figure 6b) due to electron donation by the sulfur ligands.

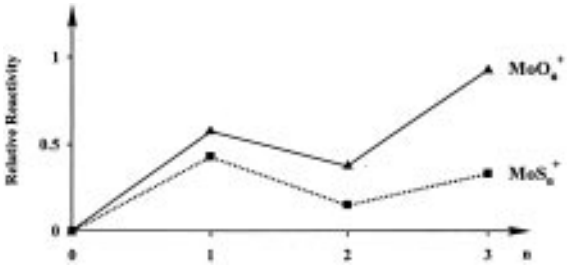

Figure 8. Relative reactivity of MoX_n^+ (X = O, S; n = 0−3) derived from the reactions with methane, ethane, benzene, and toluene. The symbols (▲) and (■) correspond to MoO_n^+ and MoS_n^+, respectively.

Further, one may expect that the IEs are in the same range of energy, with the IEs of the sulfides being smaller than the ones of the oxides, due to the higher polarizability and lower electronegativity of sulfur. Whereas this is true for the mono- and dioxides and sulfides, respectively, it is not fulfilled in the comparison of the trioxide and trisulfide species, as apparent from the IEs of MoO_3 and MoS_3 (Figure 7b). Qualitatively, this difference can be traced back to the fact that ionization from the π bond of Mo−S is much less energy demanding as compared to ionization of a Mo−O bond. By analogy, we refer to the IEs of CO_2 and COS, 13.8 and 11.2 eV, respectively,[25] which show a similar difference as do those of MoO_3 and MoS_3.

Reactivity. In order to compare the influence of ligation on reactivity, an appropriate criterion is required that accounts for the particular circumstances that prevail in the diluted gas phase. For this purpose, we have recently introduced a relative reactivity index (R), which is defined as $R = (1/i)\Sigma k_i/k_{ADO}$ for a set of reactions where i is the number of reactions examined; here, adduct formation is not considered as a reaction.[51] Thus, for a highly reactive species R is close to unity, i.e. all reactions occur at collision limit, while R approaches zero for a nonreactive species that only forms adducts. The relative reactivities of MoX_n^+ (Figure 8) show an odd/even alternation for X = O, S with Mo^+ as the least reactive species. Thus, all chalcogenide ligands enhance the reactivity as compared to the bare metal with the inert $4d^5$ configuration.

In order to rationalize the alternating trends of the MoX_n^+ ions, we must consider the requirements of bond activation. For C−H and C−C bond activation in terms of oxidative additions at least two electrons and two orbitals are necessary in order to allow for a low barrier. The monoxide and monosulfide cations possess such orbitals and have an additional intrinsic reactivity due to their three unpaired electrons. The active orbitals are located at the molybdenum center; hence, the ligands are not actively involved in the reaction and act as spectator ligands, which, nevertheless, disrupt the $4d^5$ configuration of bare Mo^+. Instead, the dioxide and disulfide cations are less reactive than MoX^+. This decrease of intrinsic reactivity of MoX_2^+ can be attributed to the fact that all but one electrons participate in strong Mo−X bonds to the ligands. As a result, the reactivity of MoX_2^+ ($^2A_1$) is smaller, because (i) only one electron is available in the doublet states, (ii) oxidative addition at the metal center would lead to unfavorable high oxidation states, and (iii) the doubly occupied orbitals that form the Mo−X bonds are rather low in energy. Following these arguments bond activation of hydrocarbons by MoX_2^+ either has to occur in a stepwise, radical-like manner involving the unpaired electron or low-lying, doubly occupied orbitals must be involved. Both scenarios are expected to give rise to high barriers and thus to low reactivities.

Hence, concerted low-energy bond activation pathways must involve a Mo−X double bond. This reasoning also accounts for the formation of neutral water in the reactions of MoO_2^+ in that oxygen is no longer a spectator ligand and actively involved in the reaction. The absence of the equivalent loss of H_2S in the reactions of MoS_2^+ can be attributed to the much lower exothermicity.

The cation-radical character is the reason for the completely new reaction pathway of hydrogen abstraction from the hydrocarbon skeleton accessible for MoX_3^+ (X = O, S). This effect is most pronounced for MoO_3^+, which is even capable of activating methane. The particular reactivity is not as marked for the molybdenum trisulfide cation. Further, the absence of any reactions, not even adduct formation, in the MoS_3^+/C_6H_6 couple indicates that the spatial requirements of the ligand environment in the trisulfide also reduce the coordination sites and thus decrease reactivity.[7]

Conclusions

The reactivity of the molybdenum cation is remarkably influenced by the number of chalcogenide ligands (X = O, S). Addition of one chalcogenide atom to Mo^+ transforms the almost inert "bare" metal center into a more reactive species. This effect can be attributed to electronic changes at the molybdenum center from a half-filled d^5 configuration of Mo^+ (^6S) to the $^4\Sigma^-$ states of MoX^+. By way of contrast, a decrease of reactivity is observed upon addition of a second chalcogenide ligand, due to the $^2A_1$ state attained in MoX_2^+ by perfect pairing of MoX^+ ($^4\Sigma^-$) and an X (^3P) atom. While the trisulfide fits in the series of MoS^+ and MoS_2^+, the third oxygen ligand in MoO_3^+ opens up completely new reaction pathways that can be attributed to the marked cation-radical character of MoO_3^+. Activation of the very strong bonds in water and methane certainly represent hallmarks in this context.

The BDEs established experimentally are in reasonable agreement with the computationally predicted BDEs. In general, the BDE of the first ligand is lower than that of the second, regardless of whether oxygen or sulfur is concerned. Relativistic effects strongly enhance the strength of the first Mo−X bond, whereas the effect is almost quenched upon addition of a second chalcogenide ligand and relativity is presumably also of minor importance for $BDE(X_2Mo^+-X)$. Nevertheless, the relatively large error bars for the experimental values render a more sophisticated evaluation of the thermochemistry of molybdenum chalcogenides highly desirable.

Acknowledgment. This research was supported by the Deutsche Forschungsgemeinschaft, the Volkswagen-Stiftung, the Fonds der Chemischen Industrie (scholarship for I.K.), and the Alexander von Humboldt-Stiftung (research fellowship for J.N.H.). We are indebted to Prof. P. E. M. Siegbahn for providing the molybdenum basis set. Furthermore, we appreciate constructive criticism by the reviewers, helpful discussions with Prof. W. Koch, Prof. P. Schwerdtfeger, Prof. S. Shaik, Dr. H. H. Cornehl, and Dipl.-Chem. T. Dargel, as well as technical support by Dr. T. Steinke.

References and Notes

(1) *Molybdenum enzymes*; Spiro, T. G., Ed.; Wiley: New York, 1985.

(2) (a) Kaim, W.; Schwederski, B. *Bioanorganische Chemie*; Teubner: Stuttgart, 1991. (b) Lippert, S. J.; Berg, J. M. *Principles of Bioinorganic Chemistry*; University Science Books: Mill Valley, CO, 1994.

(3) Andersson, A.; Hansen, S. *Catal. Lett.* **1988** *1*, 377 and references cited therein.

(4) (a) Laplaza, C. E.; Johnson, A. R.; Cummins, C. C. *J. Am. Chem. Soc.* **1996**, *118*, 709. (b) Wang, R.; Mashuta, M. S.; Richardson, J. F.; Noble, M. E. *Inorg. Chem.* **1996**, *35*, 3022. (c) Hill, J. P.; Laughlin, L. J.; Gable, R. W.; Young, C. G. *Inorg. Chem.* **1996**, *35*, 3447.

(5) (a) Huang, S.; Holman, R. W.; Gross, M. L. *Organometallics* **1986**, *5*, 1857. (b) Higashide, H.; Oka, T.; Kasatani, K.; Shinohara, H.; Sato, H. *Chem. Phys. Lett.* **1989**, *163*, 485. (c) Eller, K.; Schwarz, H. *Chem. Ber.* **1990**, *123*, 201. (d) Wesendrup, R.; Schalley, C. A.; Schröder, D.; Schwarz, H. *Chem. Eur. J.* **1995**, *1*, 608.

(6) Schilling, J. B.; Beauchamp, J. L. *Organometallics* **1988**, *7*, 194.

(7) Cassady, C. J.; McElvany, S. W. *Organometallics* **1992**, *11*, 2367.

(8) Cassady, C. J.; Weil, D. A.; McElvany, S. W. *J. Chem. Phys.* **1992**, *96*, 691.

(9) (a) Eller, K.; Schwarz, H. *Int. J. Mass Spectrom. Ion Processes* **1989**, *93*, 243. (b) Eller, K.; Zummack, W.; Schwarz, H. *J. Am. Chem. Soc.* **1990**, *112*, 621.

(10) Front-end resolution enhancement with tailored sweeps: Forbes, R. A.; Laukien, F. H.; Wronka, J. *Int. J. Mass Spectrom. Ion Processes* **1988**, *83*, 23.

(11) Su, T.; Bowers, M. T. *Int. J. Mass Spectrom. Ion Phys.* **1973**, 12, 347.

(12) Dunbar, R. C.; Uechi, G. T.; Asamoto, B. *J. Am. Chem. Soc.* **1994**, *116*, 2466.

(13) Bouchoux, G.; Salpin, J. Y.; Leblanc, D. *Int. J. Mass Spectrom. Ion Processes* **1996**, *153*, 37.

(14) (a) Schröder, D.; Fiedler, A.; Schwarz, J.; Schwarz, H. *Inorg. Chem.* **1994**, *33*, 5094. (b) Fiedler, A.; Kretzschmar, I.; Schröder, D.; Schwarz, H. *J. Am. Chem. Soc.* **1996**, *118*, 9941.

(15) Becke, A. D. *J. Chem. Phys.* **1993**, *98*, 1372.

(16) Frisch, M. J.; Trucks, G. W.; Schlegel, H. B.; Gill, P. M. W.; Johnson, B. G.; Wong, M. W.; Foresman, J. B.; Robb, M. A.; Head Gordon, M.; Replogle, E. S.; Gomperts, R.; Andres, J. L.; Ragavachari, K.; Binkley, J. S.; Gonzales, C.; Martin, R. L.; Fox, D. J.; DeFrees, D. J.; Baker, J.; Pople, J. A. *Gaussian 92/DFT; Revision F2*; Gaussian, Inc: Pittsburgh, PA, 1993.

(17) Anderson, K.; Malmquist, P.-A., III. *J. Chem. Phys.* **1988**, *92*, 2109.

(18) Andersson, K.; Fülscher, M. P.; Karlstrøm, G.; Lindh, R.; Malmqvist, P. Å.; Olsen, J.; Roos, B. J.; Sadlej, A. J.; Blomberg, M. R. A.; Siegbahn, P. E. M.; Kellø, V.; Noga, J.; Urban, M.; Widmark, P. O. *MOLCAS Version 3: AIX User's guide*; IBM: Stockholm, Sweden, 1994.

(19) Kretzschmar, I. Diploma Thesis, Technische Universität Berlin, **1996**.

(20) (a) Pyykkö, P. *Chem. Rev.* **1988**, *88*, 563. (b) Hess, B. *Ber. Bunsenges. Phys. Chem.* **1997**, *101*, 1.

(21) Dunning, T. H., Jr.; Hay, P. J. *Modern Theoretical Chemistry*; Schaefer, H. F., III, Ed.; Plenum: New York, 1976; pp 1−28.

(22) (a) Widmark, P.-O.; Malmquist, P.-Å.; Roos, B. O. *Theor. Chim. Acta* **1990**, *77*, 291. (b) Pierloot, K. ; Dunez, B.; Widmark, P.-O.; Roos, B. O. Unpublished results. (c) Pou-Amerigo, R.; Merchan, M.; Widmark, P.-O. Unpublished results.

(23) Siegbahn, P. E. M., Stockholm, Sweden. Private communication, 1995.

(24) Schmidt, M. W.; Baldridge, K. K.; Boatz, G. A.; Jensen, J. H.; Koseki, S.; Gordon, M. S.; Nguyen, K. A.; Windus, T. L.; Elbert, S. T. *QCPE Bull.* **1990**, *10*, 52.

(25) Lias, S. G.; Bartmess, J. E.; Liebman, J. F.; Holmes, J. L.; Levin, R. D.; Mallard, W. G. Gas Phase Ion and Neutral Thermochemistry. *J. Phys. Chem. Ref. Data* **1988,** *17* (Suppl. 1).

(26) Baranov, V.; Javahery, G.; Hopkinson, A. C.; Bohme, D. K. *J. Am. Chem. Soc.* **1995**, *117*, 12801.

(27) Chase, M. W.; Davies, C. A.; Downey, J. R.; Frurip, D. J.; McDonald, R. A.; Syverud, A. N. *J. Phys. Chem. Ref. Data* **1985**, *14* (Suppl. 1), 1515.

(28) Pedley, J. B.; Marshall, E. M. *J. Phys. Chem. Ref. Data* **1983**, *12*, 967.

(29) Sievers, M. R.; Chen, Y.-M.; Armentrout, P. B. *J. Chem. Phys.* **1996**, *105*, 6322.

(30) Fiedler, A.; Schröder, D.; Shaik, S.; Schwarz, H. *J. Am. Chem. Soc.* **1994**, *116*, 10734.

(31) (a) Kang, H.; Beauchamp, J. L. *J. Am. Chem. Soc.* **1986**, *108*, 7502. (b) Clemmer, D. E.; Aristov, N.; Armentrout, P. B. *J. Phys. Chem.* **1993**, *97*, 544. (c) Chen, Y.-M.; Clemmer, D. E.; Armentrout, P. B. *J. Am. Chem. Soc.* **1994**, *116*, 7815. (d) Ryan, M. F.; Fiedler, A.; Schröder, D.; Schwarz, H. *Organometallics* **1994**, *13*, 4072. (e) Ryan, M. F.; Fiedler, A.; Schröder, D.; Schwarz, H. *J. Am. Chem. Soc.* **1995**, *117*, 2033. (f) Schröder, D.; Schwarz, H.; Clemmer, D. E.; Chen, Y.; Armentrout, P. B.; Baranov, V. I.; Böhme, D. K. *Int. J. Mass Spectrom. Ion Processes* **1997**, *161*, 175.

(32) Tilson, J. L.; Harrison, J. F. *J. Phys. Chem.* **1991**, *95*, 5097; **1992**, *96*, 1667.

(33) Sugar, J.; Musgrove, A. *J. Phys. Chem. Ref. Data* **1988**, *17*, (1), 170.

(34) (a) Dyke, J. M.; Gravenor, B. W. J.; Lewis, R. A.; Morris, A. *J. Chem. Soc., Faraday Trans. 2* **1983**, *79*, 1083. (b) Harrison, J. F. *J. Phys. Chem.* **1986**, *90*, 3313. c) Jasien, P. G.; Stevens, W. J. *Chem. Phys. Lett.* **1988**, *147*, 72. (d) Schröder, D.; Schwarz, H. *Angew. Chem., Int. Ed. Engl.* **1995**, *34*, 1973.

(35) Shaik, S.; Danovich, D.; Fiedler, A.; Schröder, D.; Schwarz, H. *Helv. Chim. Acta* **1995**, *78*, 1393.

(36) (a) Siegbahn, P. E. M. *Chem. Phys. Lett.* **1993**, *201*, 15. (b) Siegbahn, P. E. M. *J. Phys. Chem.* **1993**, *97*, 9096. See also: (c) Broclawik, E. *Int. J. Quantum Chem.* **1995**, *56*, 779.

(37) Fiedler, A.; Hrušák, J.; Koch., W.; Schwarz, H. *Chem. Phys. Lett.* **1993**, *211*, 242.

(38) (a) Gunnarson, O.; Jones, R. O. *Phys. Rev. B* **1985**, *31*, 7588. (b) Ziegler, T.; Li, J. *Can. J. Chem.* **1994**, *72*, 783.

(39) Schröder, D.; Fiedler, A.; Herrmann, W. A.; Schwarz, H. *Angew. Chem., Int. Ed. Engl.* **1995**, *34*, 2517.

(40) Fischer, R. W.; Herrmann, W. A.; Bock, H.; Schröder, D.; Schwarz, H. Unpublished results.

(41) (a) Armentrout, P. B.; Halle, L. F.; Beauchamp, J. L. *J. Chem. Phys.* **1982**, *76*, 2449. (b) Plane, J. M. C. In *Gas-Phase Metal Reactions*; Fontijn, A., Ed.; Elsevier: Amsterdam, 1992; p 29. (c) Fontijn, A.; Futerko, P. M. In *Gas-Phase Metal Reactions*; Fontijn, A., Ed.; Elsevier: Amsterdam, 1992; p 109. (d) For a recent study of the reaction Mo + N_2O, see: McClean, R. E.; Campbell, M. L. Godwin, R. H. *J. Phys. Chem.* **1996**, *100*, 7502.

(42) (a) Bellert, D.; Buthelezi, T.; Lewis, V.; Dezfulian, K.; Brucat, P. J. *Chem. Phys. Lett.* **1995**, *240*, 495. (b) Heinemann, C.; Schwarz, J.; Schwarz, H. *Chem. Phys. Lett.* **1995**, *247*, 611.

(43) Baranov, V.; Bohme, D. K. *Int. J. Mass Spectrom. Ion Processes* **1995**, *149/150*, 543.

(44) Reference 7: $k_{exp} = 3.8 \times 10^{-10}$ cm^3 s^{-1}, ratio of H_2O and CH_4 losses 36:64. This work: $k_{exp} = 2.5 \times 10^{-10}$ cm^3 s^{-1}, ratio of H_2O and CH_4 losses 32:68.

(45) For a related study of OsO_4^+, see: Irikura, K. K.; Beauchamp, J. L. *J. Am. Chem. Soc.* **1989**, *11*, 75.

(46) (a) Carlin, T. J.; Wise, M. B.; Freiser, B. S. *Inorg. Chem.* **1981**, *20*, 2745. (b) Jackson, T. C.; Carlin, T. J.; Freiser, B. S. *Int. J. Mass Spectrom. Ion Processes* **1986**, *72*, 169. (c) MacMahon, T. J.; Jackson, T. C.; Freiser, B. S. *J. Am. Chem. Soc.* **1989**, *111*, 421. For a related study of MS_n^+, see: (d) Dance, I. G.; Fisher, K. J.; Willet, G. D. *Inorg. Chem.* **1996**, *35*, 4177.

(47) (a) Pestemer, M. *Angew. Chem.* **1951**, *63*, 121. (b) Houben-Weyl, *Methoden der organischen Chemie*, 4th ed.; Thieme: Stuttgart, 1955; Vol. 9, p 783.

(48) For theoretical studies of related polysulfides, see: Dance, I. G.; Fisher, K. J.; Willett, G. D. *Angew. Chem., Int. Ed. Engl.* **1995**, *34*, 201 and references therein.

(49) Bauschlicher, C. W., Jr.; Maitre, P. *Theor. Chim. Acta* **1995**, *90*, 189.

(50) Kutzelnigg, W. *Angew. Chem.* **1984**, *96*, 262 and references therein.

(51) (a) Schröder, D.; Hrušák, J.; Schwarz, H. *Ber. Bunsenges. Phys. Chem.* **1993**, *97*, 1085. (b) Cornehl, H. H.; Heinmeann, C.; Schröder, D.; Schwarz, H. *Organometallics* **1995**, *14*, 992. (c) Cornehl, H. H.; Hornung, G.; Schwarz, H. *J. Am. Chem. Soc.* **1996**, *118*, 9960.